Surface functionalization of porous In_2O_3 nanofibers with Zn nanoparticles for enhanced low-temperature NO_2 sensing properties

Chen, Kaixin; Lu, Huan; Li, Gang; Zhang, Jinniu; Tian, Yonghong; Gao, Ying; Guo, Quanmin; Lu, Hongbing; Gao, Jianzhi

DOI:
10.1016/j.snb.2020.127716

Document Version
Peer reviewed version

Citation for published version (Harvard):
Chen, K, Lu, H, Li, G, Zhang, J, Tian, Y, Gao, Y, Guo, Q, Lu, H & Gao, J 2020, 'Surface functionalization of porous In_2O_3 nanofibers with Zn nanoparticles for enhanced low-temperature NO_2 sensing properties', *Sensors and Actuators B: Chemical*, vol. 308, 127716, pp. 1-9. https://doi.org/10.1016/j.snb.2020.127716

Journal Pre-proof

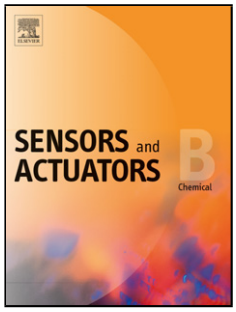

Surface functionalization of porous In_2O_3 nanofibers with Zn nanoparticles for enhanced low-temperature NO_2 sensing properties

Kaixin Chen, Huan Lu, Gang Li, Jinniu Zhang, Yonghong Tian, Ying Gao, Quanmin Guo, Hongbing Lu, Jianzhi Gao

PII: S0925-4005(20)30063-0

DOI: https://doi.org/10.1016/j.snb.2020.127716

Reference: SNB 127716

To appear in: *Sensors and Actuators: B. Chemical*

Received Date: 9 August 2019

Revised Date: 11 December 2019

Accepted Date: 13 January 2020

Please cite this article as: Chen K, Lu H, Li G, Zhang J, Tian Y, Gao Y, Guo Q, Lu H, Gao J, Surface functionalization of porous In_2O_3 nanofibers with Zn nanoparticles for enhanced low-temperature NO_2 sensing properties, *Sensors and Actuators: B. Chemical* (2020), doi: https://doi.org/10.1016/j.snb.2020.127716

Surface functionalization of porous In_2O_3 nanofibers with Zn nanoparticles for enhanced low-temperature NO_2 sensing properties

Kaixin Chen[a,1], Huan Lu[b,1], Gang Li[a], Jinniu Zhang[a], Yonghong Tian[a], Ying Gao[a], Quanmin Guo[c], Hongbing Lu[a,*] hblu@snnu.edu.cn, Jianzhi Gao[a,*] jianzhigao@snnu.edu.cn

[a] *School of Physics and Information Technology, Shaanxi Normal University, Xi'an 710062, China*

[b] *School of Geography and Tourism, Shaanxi Normal University, Xi'an, 710062, China*

[c] *School of Physics and Astronomy, University of Birmingham, Birmingham B15 2TT, United Kingdom*

[1] *These authors contributed equally to this work*

[*]Corresponding author: **Prof. Dr. Hongbing Lu**, School of Physics and Information Technology, Shaanxi Normal University, Xi'an 710062, China,

Dr. Jianzhi Gao: School of Physics and Information Technology, Shaanxi Normal University, Xi'an 710062, China,

Graphical Abstract:

Highly sensitive NO_2 sensor was constructed using porous In_2O_3 nanofibers functionalized with metal Zn nanoparticles.

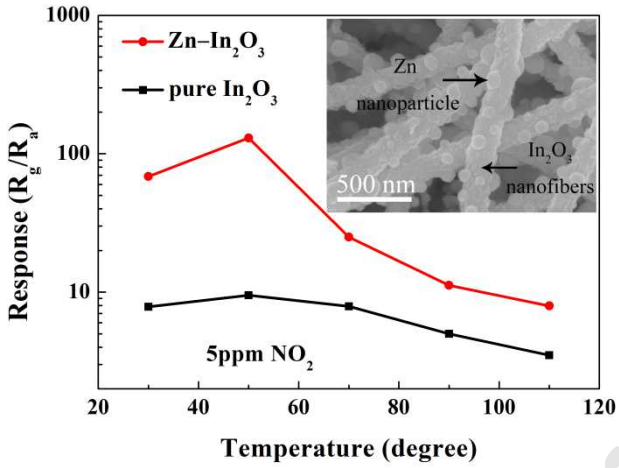

Highlights

- Metal Zn nanoparticles were decorated on the surface of In_2O_3 nanofibers.
- Zn–In_2O_3 nanofibers showed an increased surface O_2^- species absorbing capability.
- Ohmic contacts were formed between Zn nanoparticles and In_2O_3 nanoparticles.

- Zn–In_2O_3 composite nanofibers exhibited highly better NO_2 sensing performances.
- The gas sensing enhancement mechanism of Zn–In_2O_3 composite nanofibers was proposed.

Abstract

Different from the dominant method of surface modification of metal oxide sensing materials with noble metals, a simple and low-cost method is developed by using Zn nanoparticles as a surface modifier in this work. The first step involves the fabrication of porous In_2O_3 nanofibers by an electrospinning technique, and then Zn nanoparticles decorated In_2O_3 nanofibers are constructed by a simple thermal evaporation method. An increase in surface O_2^- species absorbing capability and a decrease in sensor resistance are observed by surface modification of In_2O_3 nanofibers with Zn nanoparticles. In comparison with pure In_2O_3 nanofibers, this kind of Zn–In_2O_3 composite nanofibers display higher response and better selectivity to NO_2. The response of Zn–In_2O_3 nanofibers is up to 130.00 to 5 ppm NO_2 at 50°C, which is 13.7 times higher than that of pure In_2O_3. From our perspective, the improved NO_2 sensing performances of Zn–In_2O_3 composite nanofibers are mainly attributed to the enhanced resistance modulation because of the formation of ohmic contacts between

Zn nanoparticles and In_2O_3 nanoparticles.

Keyword: Zn; In_2O_3; Nanofibers; Surface functionalization; Gas sensor

1. Introduction

Along with the development of society, frequent outbreaks of air pollution make people pay more attention to environmental protection. NO_2, an important atmospheric pollutant, is generally derived from the combustion of fuel, the emission of automobile exhaust, and the exhaust produced in industrial production. It is particularly important to monitor NO_2 using a convenient and quick method. Resistance-based metal oxide gas sensors have been widely employed to monitor NO_2 due to their fast response speed, high sensitivity, light weight, and low cost [1–3]. Among various sensing materials, In_2O_3 has wide band gap, low resistivity, and high chemical stability, showing promising sensing properties [4,5]. As for sensing application towards NO_2, In_2O_3 nanostructures with diverse morphologies have been prepared, such as nanoflowers [6], nanobelts [7], nanofibers [8], nanospheres [9], nanosheets [10,11], and nanowires [12]. Although In_2O_3 sensors have been studied intensely and some progress has been obtained, the NO_2 sensing properties of pure In_2O_3 nanostructures still require to be further improved.

Many approaches have been developed to improve sensing performances of In_2O_3, such as the formation of heterojunctions [13–15] and surface modification with noble metals [4,5,12,16–19]. Surface modification with noble metals is considered to be a universal and effective method to improve gas sensing performances of In_2O_3. For instances, Pd functionalization of In_2O_3 nanowires was synthesized by a sputtering method [18]. The sensor based on Pd–In_2O_3 nanowires exhibited an enhanced response of 4.80–5 ppm NO_2 at 300 °C [18]. Pd-loaded In_2O_3 nanowire-like networks fabricated by an electroless plating method displayed an enhanced response of 27.00–5 ppm NO_2 at 110 °C [12]. Pt nanoparticle-decorated In_2O_3 nanorods were prepared by a sol-gel method, showing a response of 11.00–200 ppm NO_2 at 300 °C [4]. Au particle-modified In_2O_3 films were prepared by a sputtering method, exhibiting an enhanced response of 28.00–10 ppm NO_2 at 400 °C [5]. Ag–In_2O_3 nanostructures fabricated by a hydrothermal method showed a response of 1.80–150 ppm NO_2 at 100 °C [19]. However, to the best of our knowledge, surface modifications of In_2O_3 nanostructures with other common metals have not been reported yet.

In this work, porous In_2O_3 nanofibers were fabricated by an electrospinning technique, and surface modification of these pre-fabricated In_2O_3 nanofibers with Zn nanoparticles was further developed by a simple thermal evaporation method. Sensing results demonstrated that Zn–In_2O_3 composite nanofibers displayed highly enhanced NO_2 sensing response in comparison with pure In_2O_3 nanofibers. The sensing enhancement mechanism of In_2O_3 nanofibers by surface functionalization with Zn

nanoparticles was also proposed. Zn–In_2O_3 composite nanofibers are selected as a research object in this work because of their following advantages: i) Nanofibers are a promising nanostructure for sensing application because of their high surface-to-volume ratio and porous structure. ii) Zn raw material is more abundant compared with noble metals. iii) Not only the increase of sensing response, but also the decrease of sensor resistance of In_2O_3 is obtained by surface modification of Zn nanoparticles. The reduced sensor resistance is in favor of the simplification of the corresponding measurement circuits, thereby benefitting the commercialization of Zn–In_2O_3 sensors.

2. Experimental

2.1 Materials

Polyvinylpyrrolidone (PVP, molecular weight of 1 300 000 g mol^{-1}) was purchased from Alfa Aesar. Indium nitrate [$In(NO_3)_3 \cdot 4.5H_2O$], zinc powder (Zn), N,N-Dimethylformamide (DMF) were purchased from Sinopharm Chemical Reagent Co, Ltd. All reagents were of analytical grade and used without further purification.

2.2 Synthesis of pure In_2O_3 nanofibers

The In_2O_3 nanofibers were synthesized by an electrospinning technique. Briefly, 0.8 g of $In(NO_3)_3 \cdot 4.5H_2O$ was firstly dissolved in a mixed solution of 8 mL of DMF and 2 mL of ethanol under magnetic stirring at room temperature. Then, 1 g of PVP was added into the above precursor solution and stirred at 60 °C for 2 h. The obtained solution was further stirred overnight at room temperature and then was transferred

into a plastic syringe for electrospinning. In the process of electrospinning, the flow rate of the solution was 1.0 mL/h. A high voltage of 18 kV and a distance of 15 cm between the needle tip and aluminum foil collector were applied. Finally, the obtained sample was placed in a muffle furnace and calcined at 500 °C in air.

2.3 Synthesis of Zn–In_2O_3 composite nanofibers

The Zn–In_2O_3 composite nanofibers were synthesized by a thermal evaporation method. High purity zinc powder (0.2 g) was spread on a corundum crucible in the upstream region of a horizontal quartz tube furnace. The pre-fabricated In_2O_3 nanofibers (0.2 g) were placed in another corundum crucible in the downstream region of the tube furnace, where the distance between Zn powder and In_2O_3 nanofibers was 30 cm. Argon with a flow rate of 80 sccm was introduced into the quartz tube. The temperatures of the Zn powder and In_2O_3 nanofibers were set to be 580 °C and 350 °C, respectively. During Zn evaporation, the total pressure in the tube furnace was maintained at 23 Torr by a mechanical pump. After 60 minutes, the system was cooled naturally to room temperature.

2.4 Characterizations

The crystal structures of samples were analyzed by X-ray diffraction (XRD: D8 Advance, Bruker, Germany) using Cu $K\alpha_1$ radiation (λ = 0.15406 nm). The scanning electron microscopy (SEM, Nova Nano-SEM450) and field emission transmission electron microscopy (TEM, Tecnai G^2 F20) were used to analyze the morphologies and structures of samples. The nitrogen adsorption and desorption measurements were carried out by a nitrogen adsorption analyzer (ASAP 2020, Micromeritics, USA) to

characterize the specific surface areas and porous structures of samples. Elemental compositions and chemical states were characterized by X-ray photoelectron spectroscopy (XPS, ESCALAB MKII, VG Scientific, UK). The ultraviolet photoelectron spectroscopy (UPS) was recorded on a monochromatic He I light source (21.2 eV) and a VG Scienta R4000 analyzer.

2.5 Fabrication and measurement of sensors

The detailed fabrication and measurement of sensors can be referred to our previous report [20,21]. In a typical process, the obtained sample was ground with appropriate amount of ethanol to form a homogeneous paste. The sensor was fabricated by painting the homogeneous paste on an Ag–Pd electrode with an active sensing area of 7 × 7 mm^2. The sensing performances were measured by a CGS-4TPs gas sensing analysis system (Elite Tech Co., Ltd, Beijing, China). The sensor was mounted on a heating ceramic plate by two probes in a sensing chamber (1.8 L). A sourcemeter was connected to the sensor through the two probes, which can be used to measure the sensor resistance in the air (R_a) and in the target gas (R_g). A micro-syringe was used to inject the target gas into the sensing chamber. The sensing response was estimated by the ratio of R_a to R_g. The response and recovery times were determined as the time taken by the response to achieve 90% of the total response change in target gas adsorption and desorption, respectively. The relative humidity (RH) for sensing tests is approximately 30% at the temperature of 25 °C.

3. Results and Discussion

Fig. 1 shows the structural features of pure In_2O_3 and Zn–In_2O_3 nanofibers measured by XRD. The diffraction pattern for pure In_2O_3 nanofibers exhibits obvious peaks at 21.5°, 30.5°, 35.5°, 50.1°, and 60.6°, corresponding to (211), (222), (400), (440), and (622) planes of cubic In_2O_3 (JCPDS card no. 65-3170), respectively. After surface decoration of In_2O_3 nanofibers with Zn nanoparticles, the obtained Zn–In_2O_3 composite nanofibers show a very similar XRD pattern with pure In_2O_3 nanofibers. All diffraction peaks for Zn–In_2O_3 nanofibers can be well indexed to cubic In_2O_3, with no Zn diffraction peaks detected. The absence of Zn diffraction peaks is probably originated from the low content and homogeneous distribution of Zn in the composite nanofibers.

The morphologies of the synthesized In_2O_3 nanofibers and Zn–In_2O_3 composite nanofibers were firstly observed by SEM. From Fig. 2(a), it is obvious that pure In_2O_3 nanofibers are randomly distributed and their sizes are relatively uniform. From the higher magnification SEM image of Fig. 2(b), the surface of pure In_2O_3 nanofibers is relatively smooth, and the average diameter is roughly 150 nm. Fig. 2(c) is the SEM image of Zn–In_2O_3 nanofibers, showing a similar morphology with pure In_2O_3. However, from the high-resolution SEM image of Fig. 2(d), it can be seen that the surface of Zn–In_2O_3 nanofibers is relatively rough. Moreover, by comparing the morphologies of pure In_2O_3 nanofibers and Zn–In_2O_3 nanofibers, it is found that the surface of Zn–In_2O_3 nanofibers is loaded with some extra nanoparticles. This is consistent with the expected experimental results that Zn nanoparticles will deposit on the surface of In_2O_3 nanofibers.

In order to examine the morphologies and detailed structural information of samples, TEM and high magnification TEM (HRTEM) measurements were performed on both pure In_2O_3 nanofibers and Zn–In_2O_3 composite nanofibers. The results of Fig. 3(a) and (b) demonstrate that pure In_2O_3 nanofibers are made up of many small nanograins. The interplanar distances of these small nanograins are measured to be approximately 0.29 nm and 0.17 nm, which match well with the (222) and (440) crystal planes of cubic phase In_2O_3, respectively. The result of Fig. 3(c) displays that some large particles with diameter of several tens of nanometers are decorated on the surface of nanofibers. The corresponding HRTEM image of a typical large particle [marked by the red circle in Fig. 3(c)] is exhibited in Fig. 3(d), where the lattice fringes can be clearly observed over the entire particle. The measured interplanar distance of the particle is about 0.21 nm, corresponding to the (101) crystal plane of hexagonal Zn (JCPDS card no. 65-3358).

XPS measurements were employed to analyze the elemental compositions and valence states of Zn–In_2O_3 nanofibers. The result of Fig. 4(a) shows the presence of In, O, Zn and C in the Zn–In_2O_3 nanofibers. The high resolution spectrum for In 3d core level peaks is exhibited in Fig. 4(b), in which two peaks at 444.07 and 451.67 eV are observed, corresponding to In $3d_{5/2}$ and In $3d_{3/2}$, respectively. The O 1s spectra of the pure In_2O_3 and Zn–In_2O_3 nanofibers are shown in Fig. 4(c) and (d), respectively. The O 1s spectra can be decomposed into two peaks, in which the one at 529.4 eV is associated with the lattice oxygen (O_L) and another one at 531.2 eV is assigned to the adsorbed oxygen (O_{ads}) [22,23]. The adsorbed oxygen ratio is further calculated to be

46.0% for Zn–In_2O_3 nanofibers, which is higher than that for pure In_2O_3 nanofibers (40.8%). This demonstrates that Zn decoration can enhance surface O_{ads} absorbing capability, which is in favor of the improvement of sensing response. The Zn 2p spectrum is displayed in Fig 4(e), where Zn $2p_{3/2}$ and $2p_{1/2}$ peaks are observed at 1021.93 and 1045.04 eV [24], respectively, indicating the metallic state of Zn element in the composite nanofibers. The relative atomic concentration of each element can be estimated using the peak areas and relative atomic sensitivity factors. The atomic concentration ratio of Zn to In is calculated to be 0.06 using the Zn $2p_{3/2}$ and In $3d_{5/2}$ signals.

N_2 adsorption–desorption measurements were used to estimate the specific surface areas and pore structures of our samples. As shown in Fig. 5(a), the adsorption–desorption curves of both pure In_2O_3 and Zn–In_2O_3 composite nanofibers exhibit type IV isotherms, suggesting the existence of abundant mesoporous structures in these nanofibers. The specific surface area of Zn–In_2O_3 is determined to be 33.8 m^2g^{-1}, which is lower than that of pure In_2O_3 (43.5 m^2g^{-1}). The pore size distribution curves of the two kinds of nanofibers are displayed in Fig. 5(b). The main pore size is centered at 3.2 nm for Zn–In_2O_3 composite nanofibers, which is almost the same as that for pure In_2O_3 nanofibers.

Sensor resistances (R_a) based on pure In_2O_3 and Zn–In_2O_3 nanofibers were also measured. Fig. 6(a) shows R_a as a function of operating temperature in the range of 30–110 °C. With the increase of temperature from 30 °C to 110 °C, the sensor resistance of pure In_2O_3 nanofibers decreases from 18160 kΩ to 670 kΩ, and that of

Zn–In_2O_3 nanofibers decreases from 521 kΩ to 30 kΩ. In comparison with pure In_2O_3 sensor, Zn–In_2O_3 sensor show much lower resistances at all measured temperatures. The response–temperature curves of the two kinds of sensors to 5 ppm NO_2 are shown in Fig. 6(b). Both sensors display an "increase-maximum-decrease" sensing characteristics. That is, the responses firstly increase with increasing operating temperature, and then reach maximum values, and finally decrease with the further increase of temperature. The optimum temperatures are determined to be 50 °C for both pure In_2O_3 and Zn–In_2O_3 nanofibers. Especially, at all measured temperatures ranging from 30 to 110 °C, the responses of Zn–In_2O_3 nanofibers are higher than those of pure In_2O_3 nanofibers. For an example, when the temperature is 50°C, the response of Zn–In_2O_3 nanofibers is as high as 130.00, which is about 13.7 times higher than that of pure In_2O_3.

Fig. 7(a) and (b) show the dynamic response–recovery curves of the two kinds of sensors at NO_2 concentration ranges of 2–10 ppm and 50–1000 ppb, respectively. Obviously, as the concentration of NO_2 increases, the response increases for the two kinds of sensors. When the concentrations of NO_2 are 50 ppb, 100 ppb, 500 ppb, 800 ppb, 1000 ppb, 2 ppm, 5 ppm, and 10 ppm, the responses of Zn–In_2O_3 sensor are 1.26, 1.51, 2.38, 4.18, 7.34, 21.00, 130.00, and 248.20, while those of pure In_2O_3 sensor are 1.22, 1.28, 1.33, 1.58, 2.71, 3.50, 9.50, and 19.50, respectively. The above results indicate that the Zn–In_2O_3 and In_2O_3 sensors can detect a low-concentration NO_2 of 50 ppb. The response–recovery curves to 5 ppm NO_2 at 50 °C are used to determine the response and recovery times of the two kinds of sensors, as shown in Fig. S1 in

the Supplementary Material. The response and recovery times of pure In_2O_3 sensor are 496 s and 3131 s, and those of Zn–In_2O_3 sensor are 600 s and 2218 s, respectively. The recovery times of the two sensors are relatively long, which are consistent with previously-reported values of metal oxide-based NO_2 sensors [25,26]. The relatively long recovery times of the two sensors are mainly attributed to the slow desorption rate of NO_2 molecules on the surfaces of In_2O_3 and Zn–In_2O_3 nanofibers at low operating temperatures.

Fig. 8 shows the selectivity measurement of the Zn–In_2O_3 sensor to NO_2 against various interfering gases at the temperature of 50 °C, where the concentration of NO_2 is 5 ppm and the concentration of interfering gases is 100 ppm. It can be seen that the responses of pure In_2O_3 and Zn–In_2O_3 sensors are 9.50 and 130.00 to 5 ppm NO_2, respectively, while the responses of the two sensors are less than 2.10 to 100 ppm interfering gases, such as ethanol, toluene, acetone, and acetic acid. Therefore, the two kinds of sensors, especially the Zn–In_2O_3 sensor, exhibit good sensing selectivity to NO_2. It should be pointed out that although ethanol is an inflammable gas, a response of 2.10 is still obtained for pure In_2O_3 sensor. Good ethanol sensing responses based on metal oxide-based sensors at high temperatures (≥ 300 °C) have been revealed in some previous reports [27,28]. We think that no flaming of ethanol occurs in our case since the ethanol concentration in the sensing chamber is very low and the operating temperature is much lower than the ignition point of ethanol.

The effect of RH on the response properties of pure In_2O_3 and Zn–In_2O_3 sensors was also studied, as exhibited in Fig. 9. Both sensors display a visible decrease in NO_2

response with the increase of RH from 30% to 75%. This phenomenon can be ascribed to the following reasons. Firstly, under high RH, more water molecules are adsorbed on the surfaces of In_2O_3 and Zn–In_2O_3 nanofibers, resulting in the decreased adsorption of NO_2 molecules. Secondly, the sensing reaction between NO_2 molecules and adsorbed oxygen species is also suppressed by the reaction between adsorbed water molecules and adsorbed oxygen species [29]. Nevertheless, the Zn–In_2O_3 sensor still displays a relativity high response of 31.10 even at a high RH of 75%.

A comparison of the NO_2 sensing performances was also performed between Zn–In_2O_3 nanofibers and previously reported In_2O_3-based nanostructures, as shown in Table 1 [4,5,12,15,18,19,30–34]. It is seen that the Zn–In_2O_3 nanofibers in this work display relatively higher NO_2 response and lower operating temperature than some of the reported noble metals modified In_2O_3 and In_2O_3-based heterojunction nanostructures [4,5,12,15,18,19,34], although the response of our sensor is lower than several reported In_2O_3-based sensors [30–33]. Additionally, the Zn–In_2O_3 sensor exhibits good NO_2 selectivity and relatively high response to NO_2 under high RH. Therefore, our sensor is still a promising candidate for application in sensitive detection of NO_2 at low operating temperature.

4. Sensing mechanism

Generally, the sensing mechanism of In_2O_3 nanofibers is controlled by a chemisorbed oxygen-related resistance modulation model [35–37]. When the In_2O_3 nanofiber-based sensor is placed in air, O_2 molecules in air are adsorbed on the

surfaces of In_2O_3 nanofibers, forming chemisorbed oxygen species (O_2^-) by occupying the electrons in the conduction band of In_2O_3, as described by Eqs. (1) and (2).

$$O_{2(gas)} \rightarrow O_{2(ads)} \quad (1)$$

$$O_{2(ads)} + e^- \rightarrow O^-_{2(ads)} \quad (2)$$

When NO_2 molecules are introduced, owing to their electrophilic property, the NO_2 molecules not only occupy the e^- in the conduction band of In_2O_3 [Eq. (3)], but also interact with the $O^-_{2(ads)}$ species through Eq. (4) [38–41]. These two reactions can occur simultaneously. The above two processes will consume a large number of e^- in the conduction band of In_2O_3, leading to a high resistance state of the sensor upon the introduction of NO_2.

$$NO_{2(gas)} + e^- \rightarrow NO^-_{2(ads)} \quad (3)$$

$$NO_{2(gas)} + O^-_{2(ads)} + 2e^- \rightarrow NO^-_{2(ads)} + 2O^-_{(ads)} \quad (4)$$

The sensing results demonstrate the enhanced NO_2 sensing performances of Zn–In_2O_3 nanofibers. The BET results show that Zn–In_2O_3 nanofibers possess lower surface area and similar pore structure in comparison with pure In_2O_3 nanofibers. These indicate that the enhanced NO_2 sensing performances of Zn–In_2O_3 nanofibers are not originated from their specific surface area and pore structure. From our viewpoint, the enhanced resistance modulation because of the formation of ohmic contacts between Zn nanoparticles and In_2O_3 nanoparticles contributes greatly to the improved NO_2 sensing performances of Zn–In_2O_3 nanofibers. In order to determine the electron transfer direction between Zn and In_2O_3 nanoparticles, the work functions for the pure In_2O_3 and Zn–In_2O_3 nanofibers were estimated by UPS spectra [42]. The

UPS spectra indicate that the high binding energy cutoff values for pure In_2O_3 nanofibers [Fig. 10(a)] and Zn–In_2O_3 nanofibers [Fig. 10(b)] are 17.01 eV and 17.13 eV, respectively. The work functions of pure In_2O_3 nanofibers and Zn–In_2O_3 nanofibers are thus determined to be 4.19 eV and 4.07 eV, respectively. The above results also indicate that the work function of Zn nanoparticles is smaller than that of pure In_2O_3 nanofibers. In other words, the Fermi level of Zn is higher than that of In_2O_3, as illustrated by the schematic energy band diagram in Fig. 11(a). When Zn nanoparticles contact with In_2O_3 nanoparticles, ohmic contacts are generated at the interfaces between Zn nanoparticles and In_2O_3 nanoparticles. The electron transfer from Zn to In_2O_3 nanoparticles occurs, and finally an equilibrium of Fermi levels between Zn and In_2O_3 is reached, as displayed by the schematic energy band diagram in Fig. 11(b). The above process leads to the reduced electron depletion layer of In_2O_3 nanofibers. As shown in Fig. 6(a), R_a values are 12600 kΩ and 379 kΩ based on pure In_2O_3 nanofibers and Zn–In_2O_3 nanofibers, respectively. This decrease in sensor resistance of Zn–In_2O_3 nanofibers confirms the electron transfer direction from Zn to In_2O_3 nanoparticles and the formation of ohmic contacts. Since the transferred electrons in the conduction band of In_2O_3 are active, more chemisorbed O_2^- ions are produced through Eq. (2) [13,43]. XPS results in Fig. 4(c) also demonstrate this increase in chemisorbed O_2^- capability of Zn–In_2O_3 nanofibers. To clarify the influence of O_{ads} absorbing capability on the sensing response of our sensors, R_a and response–recovery curves of the Zn–In_2O_3 sensor at 50 °C under various O_2 concentrations were measured. The background gases with various O_2 concentrations

were acquired by mixing O_2 and Ar with required proportions. The result in Fig. 12(a) shows that R_a increases with the increase of O_2 concentrations in the tested range (0%–29.0%). This result is reasonable since more O_2 molecules are absorbed on the surfaces of Zn–In_2O_3 nanofibers and more electrons in the conduction band of In_2O_3 are occupied through Eq. (2) under higher O_2 concentration. The result in Fig. 12(b) shows that the NO_2 response increases with the increase of O_2 concentration. The above results indicate that high O_{ads} absorbing capability can undoubtedly enhance the NO_2 response of Zn–In_2O_3 sensor. As described by Eqs. (3) and (4), a NO_2 molecule can exhaust one electron through the reaction of Eq. (3), while a NO_2 molecule can exhaust two electrons through the reaction of Eq. (4). Therefore, higher O_{ads} absorbing capability can lead to a larger change of resistance by exhausting more electrons through the reaction between NO_2 molecules and $O^-_{2(ads)}$. As a result, the Zn–In_2O_3 nanofibers with higher $O^-_{2(ads)}$ capability have higher NO_2 sensing response compared with pure In_2O_3 nanofibers.

5. Conclusions

In summary, porous In_2O_3 nanofibers are fabricated by an electrospinning technique, and surface modification of these pre-fabricated In_2O_3 nanofibers with Zn nanoparticles is further developed by a simple thermal evaporation method. By Zn nanoparticle surface modification, the surface O^-_2 species absorbing capability of In_2O_3 nanofibers is increased and In_2O_3 sensor resistance is decreased. Sensing results demonstrate that Zn–In_2O_3 composite nanofibers exhibit highly enhanced NO_2

sensing response in comparison with pure In_2O_3 nanofibers. The response of Zn–In_2O_3 nanofibers is up to 130.00 to 5 ppm NO_2 at 50°C, which is 13.7 times as high as that of pure In_2O_3. Additionally, the Zn–In_2O_3 nanofibers also display excellent selectivity and low detection limit towards NO_2. By surface modification of In_2O_3 nanofibers with Zn nanoparticles, ohmic contacts between Zn nanoparticles and In_2O_3 nanoparticles are generated, contributing greatly to the enhanced resistance modulation capability and enhanced NO_2 sensing responses of Zn–In_2O_3 nanofibers. Our results suggest that this kind of Zn–In_2O_3 nanofibers is a promising candidate for sensitive and selective NO_2 detection. The simple and low-lost method developed in this work can be easily extended to construct metal nanoparticles modified metal oxide nanostructures with high sensing performances.

Declaration of interests

The authors declare that they have no known competing financial interests or personal relationships that could have appeared to influence the work reported in this paper.

Acknowledgements

This work was supported by the National Natural Science Foundation of China (Nos. 11574189 and 11604196), the Science and Technology Program of Shaanxi Province (Nos. 2019JM-102 and 2016KJXX-15), and the Fundamental Research Funds for the Central Universities (Nos. GK201602006, GK201801005, and 2018CBLZ002). This work was also supported by the National Demonstration Center for Experimental X-physics Education of Shaanxi Normal University.

References

[1] Y.S. Liu, X.P. Liu, Y.B. Wang, R. Wang, T. Zhang, Metal-organic-framework-derived In_2O_3 microcolumnar structures embedded with Pt nanoparticles for NO_2 detection near room temperature, Ceram. Int. 45 (2019) 9820–9828.

[2] V. Annapureddy, Y.H. Kim, G.T. Hwang, H.W. Jang, S.D. Kim, J.J. Choi, B.J. Cho, J.H. Ryu, Room-temperature solid-state grown $WO_{3-\delta}$ film on plastic substrate for extremely sensitive flexible NO_2 gas sensors, Adv. Mater. Interfaces 5 (2018) 1700811–1700818.

[3] Y.S. Haiduk, A.A. Khort, N.M. Lapchuk, A.A. Savitsky, Study of WO_3–In_2O_3 nanocomposites for highly sensitive CO and NO_2 gas sensors, J. Solid State Chem. 273 (2019) 25–31.

[4] S.B. Choi, J.K. Lee, W.S. Lee, T.G. Ko, C. Lee, Optimization of the Pt nanoparticle size and calcination temperature for enhanced sensing performance of Pt-decorated In_2O_3 nanorods, J. Korean Phys. Soc. 10 (2018) 1444–1451.

[5] H. Steffes, C. Imawan, F. Solzbacher, E. Obermeier, Enhancement of NO_2 sensing properties of In_2O_3-based thin films using an Au or Ti surface modification, Sens. Actuators B 78 (2001) 106–112.

[6] X.M. Xu, H.J. Zhang, X.L. Hu, P Sun, Y.S. Zhu, C.Z. He, S.J. Hou, Y.F. Sun, G.Y. Lu, Hierarchical nanorod–flowers indium oxide microspheres and their gas sensing

properties, Sens. Actuators B 227 (2016) 547–553.

[7] H. Kim, S. An, C. Jin, C. Lee, Structure and NO_2 gas sensing properties of SnO_2-core/In_2O_3-shell nanobelts, Curr. Appl. Phys. 12 (2012) 1125–1130.

[8] Y.S. Liu, X. Gao, F. Li, G.Y. Lu, T. Zhang, N. Barsan, Pt–In_2O_3 mesoporous nanofibers with enhanced gas sensing performance towards ppb-level NO_2 at room temperature, Sens. Actuators B 260 (2018) 927–936.

[9] B.X. Xiao, D.X. Wang, S.L. Song, C.B. Zhai, F. Wang, M.Z. Zhang, Fabrication of mesoporous In_2O_3 nanospheres and their ultrasensitive NO_2 sensing properties. Sens. Actuators B 248 (2017) 519–526.

[10] X. Wang, J. Su, H. Chen, G.D. Li, Z.F. Shi, H.F. Zou, X.X. Zou, Ultrathin In_2O_3 nanosheets with uniform mesopores for highly sensitive nitric oxide detection, ACS Appl. Mater. Interfaces 9 (2017) 16335–16342.

[11] B.X. Xiao, S.L. Song, P. Wang, Q. Zhao, M.Y. Chuai, M.Z. Zhang, Promoting effects of Ag on In_2O_3 nanospheres of sub-ppb NO_2 detection, Sens. Actuators B 241 (2017) 489–497.

[12] M.Q. Huang, Z.D. Cui, X.J. Yang, S.L. Zhu, Z.Y. Li, Y.Q. Liang, Pd-loaded In_2O_3 nanowire-like network synthesized using carbon nanotube templates for enhancing NO_2 sensing performance, RSC Adv. 5 (2015) 30038–30045.

[13] G. Li, X. Zhang, H. Lu, C. Yan, K.X. Chen, H.B. Lu, J.Z. Gao, Z.B. Yang, G.Q. Zhu, C.L. Wang, Z. He, Ethanol sensing properties and reduced sensor resistance using porous Nb_2O_5–TiO_2 n–n junction nanofibers, Sens. Actuators B 283 (2019) 602–612.

[14] Z.B. Dong, S.T. Liu, In_2O_3-decorated ordered mesoporous NiO for enhanced NO_2 sensing at room temperature, J. Mater. Sci. Mater. Electron. 29 (2018) 2645-2653.

[15] D.Z. Zhang, D. Wu, Y.H. Cao, X.Q. Zong, Z.M. Yang, Construction of Co_3O_4 nanorods/In_2O_3 nanocubes heterojunctions for efficient sensing of NO_2 gas at low temperature, J. Mater. Sci. Mater. Electron. 29 (2018) 19558–19566.

[16] B.Y. Huang, Y.R. Wang, Q. Hu, X.M. Mu, Y.X. Zhang, J.L. Bai, Q. Wang, Y.Z. Sheng, Z.X. Zhang, E.Q. Xie, A low temperature and highly sensitive ethanol sensor based on Au modified In_2O_3 nanofibers by coaxial electrospinning, J. Mater. Chem. C 6 (2018) 10935–10943.

[17] S. Zhang, P. Song, J. Zhang, H.H. Yan, J. Li, Z.X. Yang, Q. Wang, Highly sensitive detection of acetone using mesoporous In_2O_3 nanospheres decorated with Au nanoparticles, Sens. Actuators B 242 (2017) 983–993.

[18] S.S. Kim, J.Y. Par, S.W. Choi, H.G. Na, J.C. Yang, H.W. Kim, Enhanced NO_2 sensing characteristics of Pd-functionalized networked In_2O_3 nanowires, J. Alloys Compd. 509 (2011) 9171–9177.

[19] R.S. Sabry, I.R. Agool, A.M. Abbas, Hydrothermal synthesis of In_2O_3: Ag nanostructures for NO_2 gas sensor, Silicon 10 (2018) 1–4.

[20] X. Xin, J.N. Zhang, C.J. Chen, G. Li, J. Qin, Z.B. Yang, H.B. Lu, J.Z. Gao, C.L. Wang, Z. He, UV-activated porous Zn_2SnO_4 nanofibers for selective ethanol sensing at low temperatures, J. Alloys. Compd. 780 (2019) 228–236.

[21] J.N. Zhang , H.B. Lu, C. Liu, C.J. Chen, X. Xin, Porous NiO–WO_3

heterojunction nanofibers fabricated by electrospinning with enhanced gas sensing properties, RSC Adv. 7 (2017) 40499–40509.

[22] C. Yan, H.B. Lu, J.Z. Gao, G.Q. Zhu, F. Yin, Z.B. Yang, Q.R. Liu, G. Li, Synthesis of porous NiO–In_2O_3 composite nanofibers by electrospinning and their highly enhanced gas sensing properties, J. Alloys Compd. 699 (2017) 567–574.

[23] V.G. Krishnan, A. Purushothaman, P. Elango, A study of the physical properties and gas-sensing performance of TiO_2 nanofilms: Automated nebulizer spray pyrolysis method (ANSP), Phys. Status Solidi A 214 (2017) 1–9.

[24] R. Ramarajan, M. Kovendhan, P. Duy-Thach, K. Thangaraju, R. Ramesh Babu, J. Ki-Joon, D. Paul Joseph, Optimization of Zn_2SnO_4 thin film by post oxidation of thermally evaporated alternate Sn and Zn metallic multi-layers, Appl. Surf. Sci. 449 (2018) 68–76.

[25] P.G. Su, T.T. Pan, Fabrication of a room-temperature NO_2 gas sensor based on WO_3 films and WO_3/MWCNT nanocomposite films by combining polyol process with metal organic decomposition method, Mater. Chem. Phys. 125 (2011) 351–357.

[26] F. Gu, R. Nie, D. Han, Z. Wang, In_2O_3–graphene nanocomposite based gas sensor for selective detection of NO_2 at room temperature, Sens. Actuators B 219 (2015) 94–99.

[27] D.R. Miller, S.A. Akbar, P.A. Morris, Nanoscale metal oxide-based heterojunctions for gas sensing: a review, Sens. Actuators B 204 (2014) 250–272.

[28] T.M. Li, W. Zeng, Z.C. Wang, Quasi-one-dimensional metal-oxide-based heterostructural gas-sensing materials: a review, Sens. Actuators B 221 (2015)

1570–1585.

[29] D. Koziej, N. Barsan, U. Weimar, J. Szuber, K. Shimanoe, N. Yamazoe, Water–oxygen interplay on tin dioxide surface: implication on gas sensing, Chem. Phys. Lett. 410 (2005) 321–323.

[30] D.M. Han, L.L. Zhai, F.B. Gu, Z.H. Wang, Highly sensitive NO_2 gas sensor of ppb-level detection based on In_2O_3 nanobricks at low temperature, Sens. Actuators B 262 (2018) 655–663.

[31] Y.S. Liu, X. Gao, F. Li, G.Y. Lu, T. Zhang, N. Barsan, Pt–In_2O_3 mesoporous nanofibers with enhanced gas sensing performance towards ppb-level NO_2 at room temperature, Sens. Actuators B 260 (2018) 927–936.

[32] T. Ueda, K. Ishida, K. Kamada, T. Hyodo, Y. Shimizu, Improvement in NO_2 sensing properties of semiconductor-type gas sensors by loading of Au into porous In_2O_3 powders, Front. Mater. 81 (2019) 1–10.

[33] Z.H. Wang, G.L. Men, R.X. Zhang, F.B. Gu, D.M. Han, Pd loading induced excellent NO_2 gas sensing of 3DOM In_2O_3 at room temperature, Sens. Actuators B 263 (2018) 218–228.

[34] C. Yan, H.B. Lu, J.Z. Gao, Y. Zhang, Q.M. Guo, H.X. Ding, Y.T. Wang, F.F. Wei, G.Q. Zhu, Z.B. Yang, C.L. Wang, Improved NO_2 sensing properties at low temperature using reduced graphene oxide nanosheet–In_2O_3 heterojunction nanofibers, J. Alloys Compd. 741 (2018) 908–917.

[35] Z.H. Jing, J.H. Zhan, Fabrication and gas-sensing properties of porous ZnO nanoplates, Adv. Mater. 20 (2008) 4547–4551.

[36] J.N. Zhang, H.B. Lu, C. Yan, Z.B. Yang, G.Q. Zhu, J.Z. Gao, F. Yin, C.L. Wang, Fabrication of conductive graphene oxide–WO_3 composite nanofibers by electrospinning and their enhanced acetone gas sensing properties, Sens. Actuators B 264 (2018) 128–138.

[37] M.L. Yin, S.Z. Liu, Controlled ZnO hierarchical structure for improved gas sensing performance, Sens. Actuators B 209 (2015) 343–351.

[38] T.T. Wang, J.Y. Hao, S.L. Zheng, Q. Sun, D. Zhang, Y. Wang, Highly sensitive and rapidly responding room-temperature NO_2 gas sensors based on WO_3 nanorods/sulfonated graphene nanocomposites. Nano Res. 11 (2018) 791–803.

[39] S.L. Bai, D.Q. Li, D.M. Han, R.X. Luo, A.F. Chen, C.C. Liu, Preparation, characterization of WO_3–SnO_2 nanocomposites and their sensing properties for NO_2, Sens. Actuators B 150 (2010) 749–755.

[40] Z.B. Wang, D. Wang, J.B. Sun, Controlled synthesis of defect-rich ultrathin two-dimensional WO_3 nanosheets for NO_2 gas detection, Sens. Actuators B 245 (2017) 828–834.

[41] S.L. Bai, K.W. Zhang, R.X. Luo, D.Q. Li, A.F. Chen, C.C. Liu, Low-temperature hydrothermal synthesis of WO_3 nanorods and their sensing properties for NO_2, J. Mater. Chem. 22 (2012) 12643–12650.

[42] J.N. Zhang, H. Lu, H.B. Lu, G. Li, J.Z. Gao, Z.B. Yang, Y.H. Tian, M. Zhang, C.L. Wang, Z. He, Porous bimetallic Mo–W oxide nanofibers fabricated by electrospinning with enhanced acetone sensing performances, J. Alloys Compd. 779 (2019) 531–542.

[43] W. Zeng, T.M. Liu, Z.C. Wang, Sensitivity improvement of TiO_2-doped SnO_2 to volatile organic compounds, Phys. E 43 (2010) 633–638.

Author Biographies

Kaixin Chen received his B.S. degree from Shanxi Normal University in 2017. He is currently a M.Sc. student in School of Physics and Information Technology, Shaanxi Normal University, China. He is interested in the preparation and sensing application of semiconductor oxides.

Huan Lu is a lecturer of Shaanxi Normal University, China. She is interested in environment applications of nanomaterials.

Gang Li received his B.S. degree in 2017 from Shaanxi Normal University. He is now a M.Sc. candidate in School of Physics and Information Technology, Shaanxi Normal University. His research interest is the preparation and sensing application of semiconductor oxides.

Jinniu Zhang received his B.S. degree from Northwest Normal University in 2015. He is currently a Ph.D. student in School of Physics and Information Technology, Shaanxi Normal University, China. His research interests include the synthesis of oxide nanomaterials and their application in gas sensors.

Yonghong Tian received her B.S. degree from Xinzhou Teachers University in 2017. She is currently a M.Sc. student in School of Physics and Information Technology, Shaanxi Normal University, China. She is interested in the synthesis and characterization of nanomaterials.

Ying Gao received her B.S. degree from Lanzhou Jiaotong University in 2018. She is currently a M.Sc. student in School of Physics and Information Technology, Shaanxi Normal University, China. Her research interest is the preparation and application of semiconductor oxides.

Quanmin Guo received his Ph.D. degree in 1989 from Lancaster University, United Kingdom. He is currently working as a professor of University of Birmingham, United Kingdom. He is interested in the synthesis and characterization of nanomaterials.

Hongbing Lu received his Ph.D. degree in 2009 from Wuhan University, China. He is currently working as a professor of Shaanxi Normal University. His research interests include nanomaterials and chemical sensors.

Jianzhi Gao received his Ph.D. degree in 2013 from University of Birmingham, United Kingdom. He is currently working as an associate professor of Shaanxi Normal University. He is interested in the synthesis and characterization of nanomaterials.

Figure Captions

Fig. 1

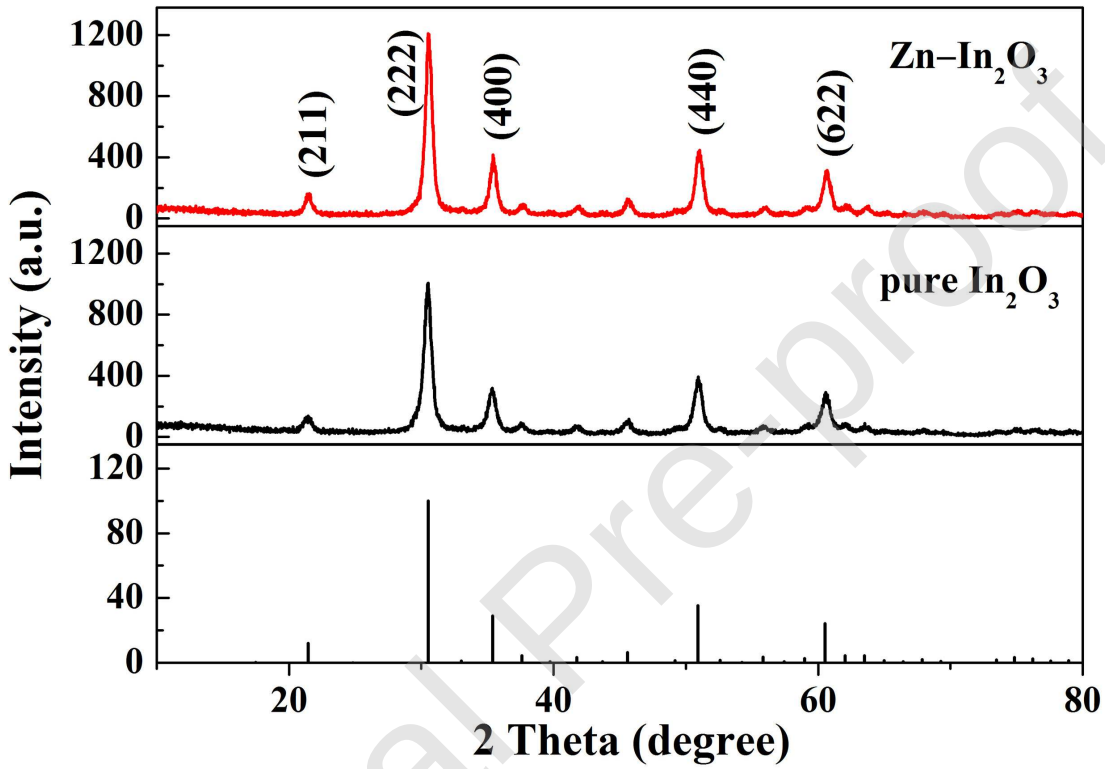

1. **Fig. 1**. XRD patterns of pure In_2O_3 and Zn–In_2O_3 composite nanofibers.

Fig. 2

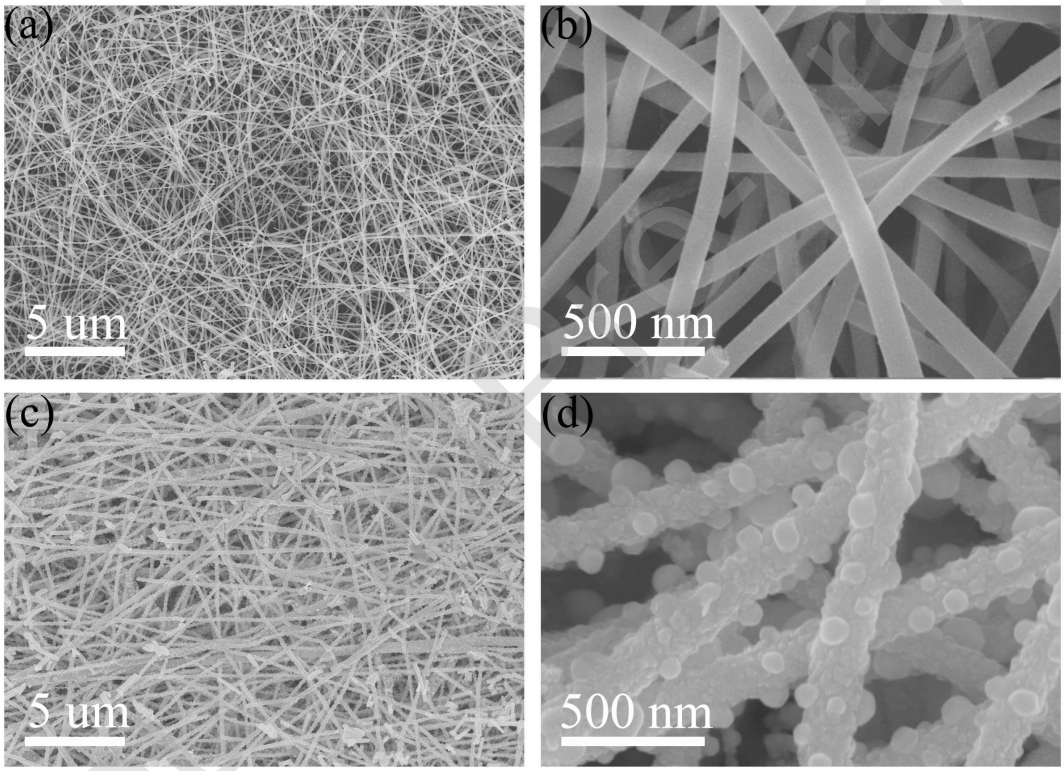

2. **Fig. 2**. SEM images of (a) pure In_2O_3 nanofibers and (c) Zn–In_2O_3 composite nanofibers; (b) and (d) are the corresponding high magnification SEM images of pure In_2O_3 nanofibers and Zn–In_2O_3 composite nanofibers, respectively.

Fig. 3

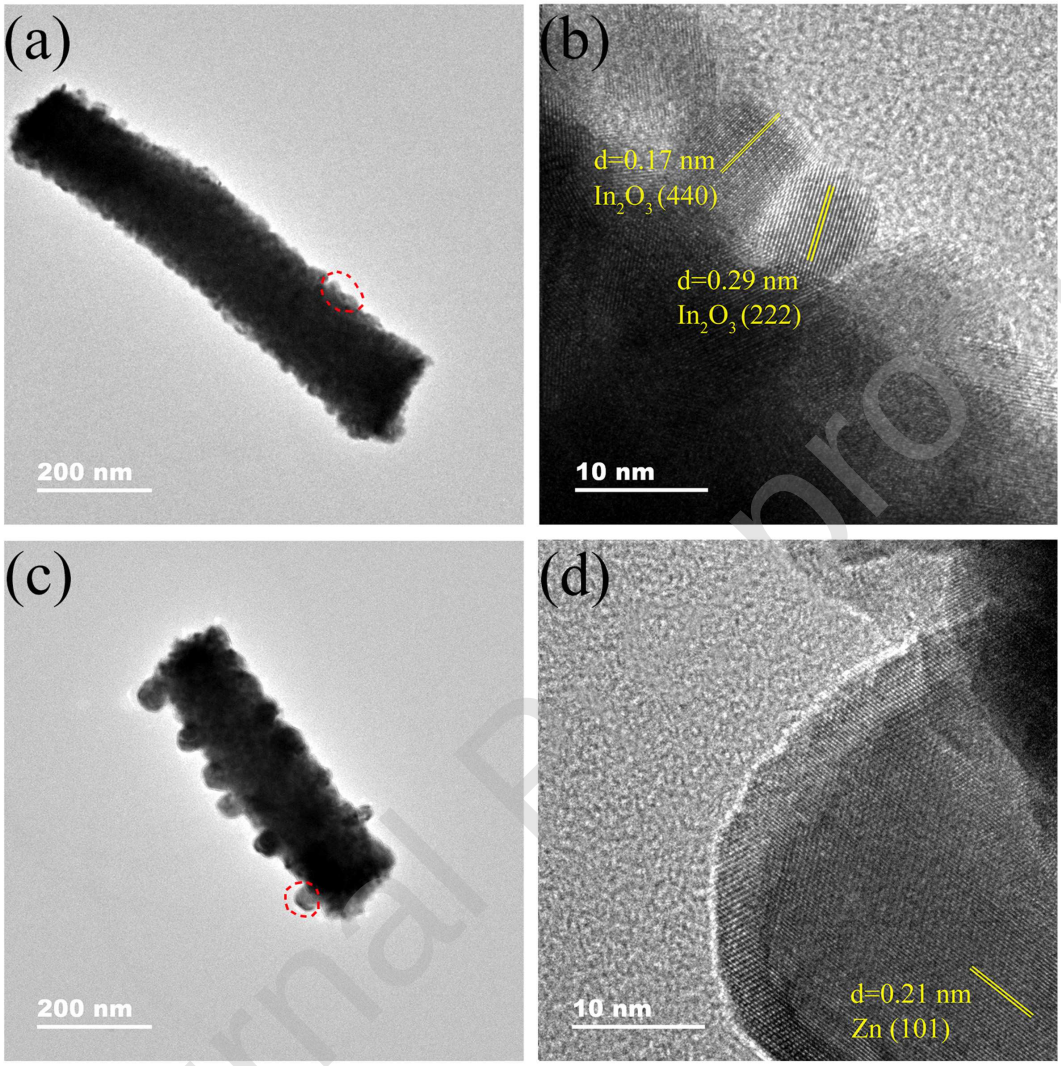

3. Fig. 3. TEM images of (a) pure In_2O_3 and (c) Zn–In_2O_3 composite nanofibers; (b) and (d) are the corresponding HRTEM patterns of pure In_2O_3 and Zn–In_2O_3

composite nanofibers, respectively.

Fig. 4

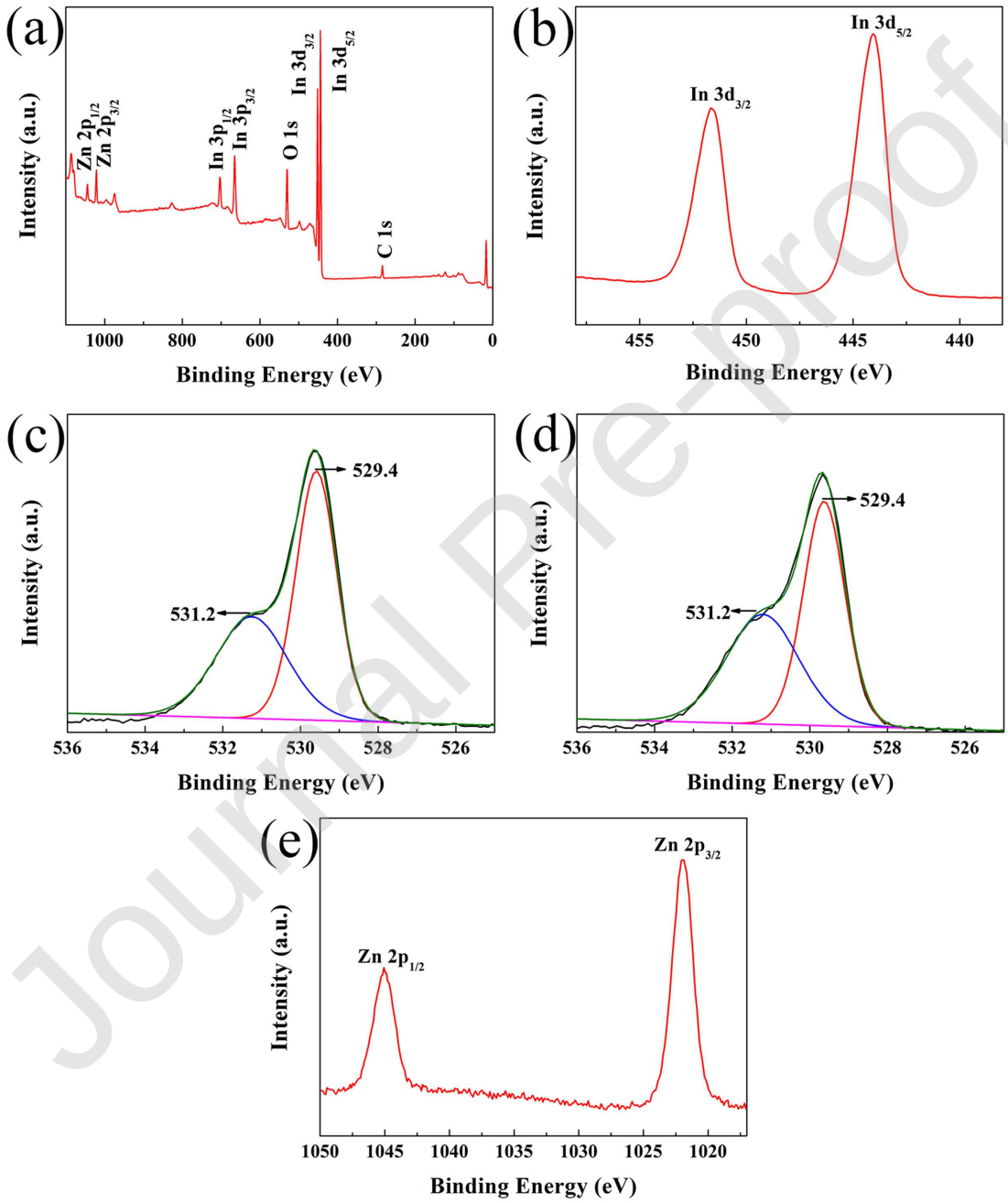

4. **Fig. 4**. (a) Survey spectrum and (b) high resolution spectrum for In 3d of Zn–In_2O_3 composite nanofibers; high resolution spectra for O 1 s of (c) pure In_2O_3 and (d) Zn–In_2O_3 composite nanofibers; (e) high resolution spectrum for Zn 2p of Zn–In_2O_3 composite nanofibers.

Fig. 5

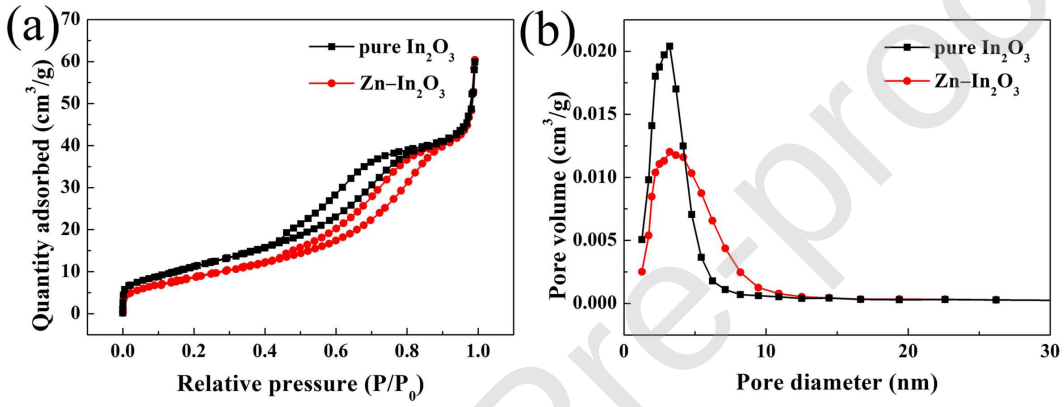

5. **Fig. 5**. (a) Nitrogen adsorption–desorption isotherms and (b) the corresponding

pore-size distribution curves of pure In_2O_3 and Zn–In_2O_3 composite nanofibers.

Fig. 6

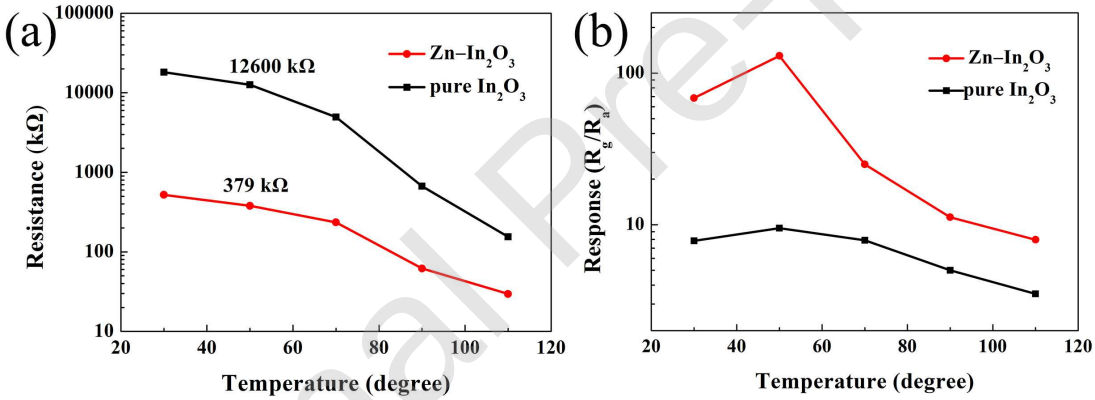

6. **Fig. 6**. (a) Resistances in air of the two kinds of sensors at various temperatures; (b) responses of the two kinds of sensors to 5 ppm NO_2 at various temperatures.

Fig. 7

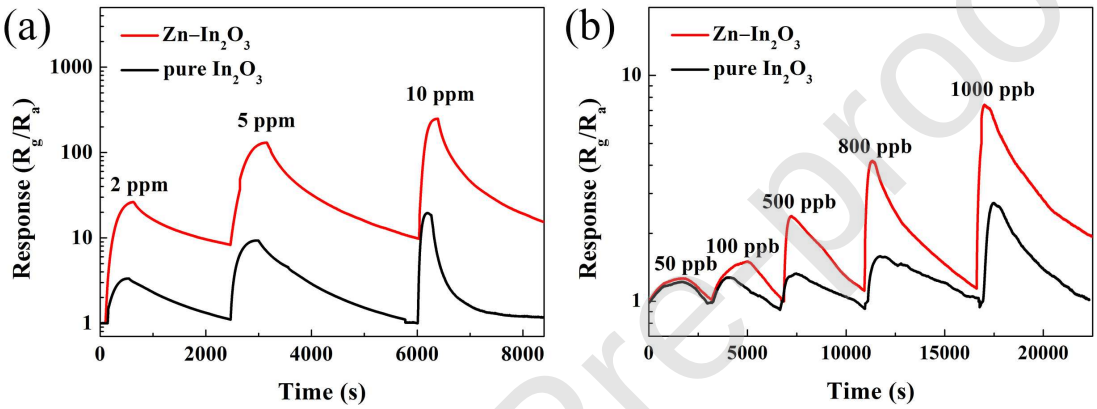

7. Fig. 7. Response–time curves of the sensors based on pure In_2O_3 and Zn–In_2O_3 nanofibers to various NO_2 concentrations at 50 °C: (a) 2–10 ppm and (b) 50–1000

ppb.

Fig. 8

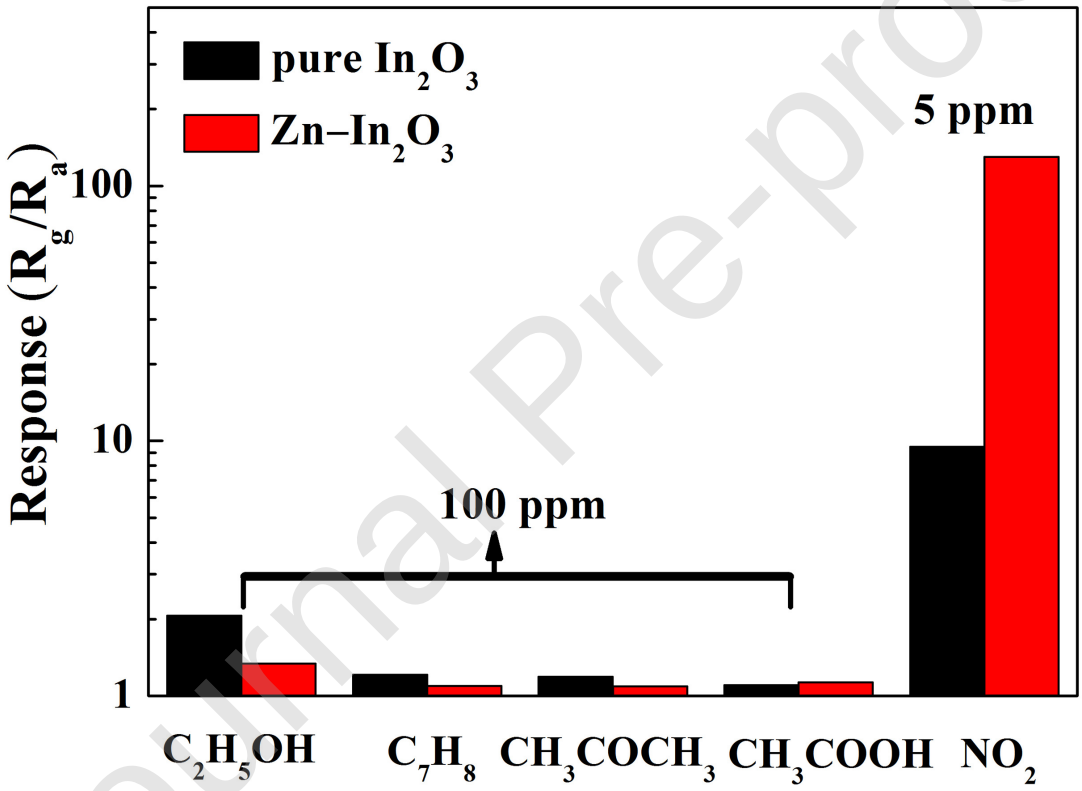

8. **Fig. 8**. Sensing responses of the sensors based on pure In_2O_3 and Zn–In_2O_3 nanofibers toward NO_2 (5 ppm) against other interfering gases (100 ppm) at 50 °C.

Fig. 9

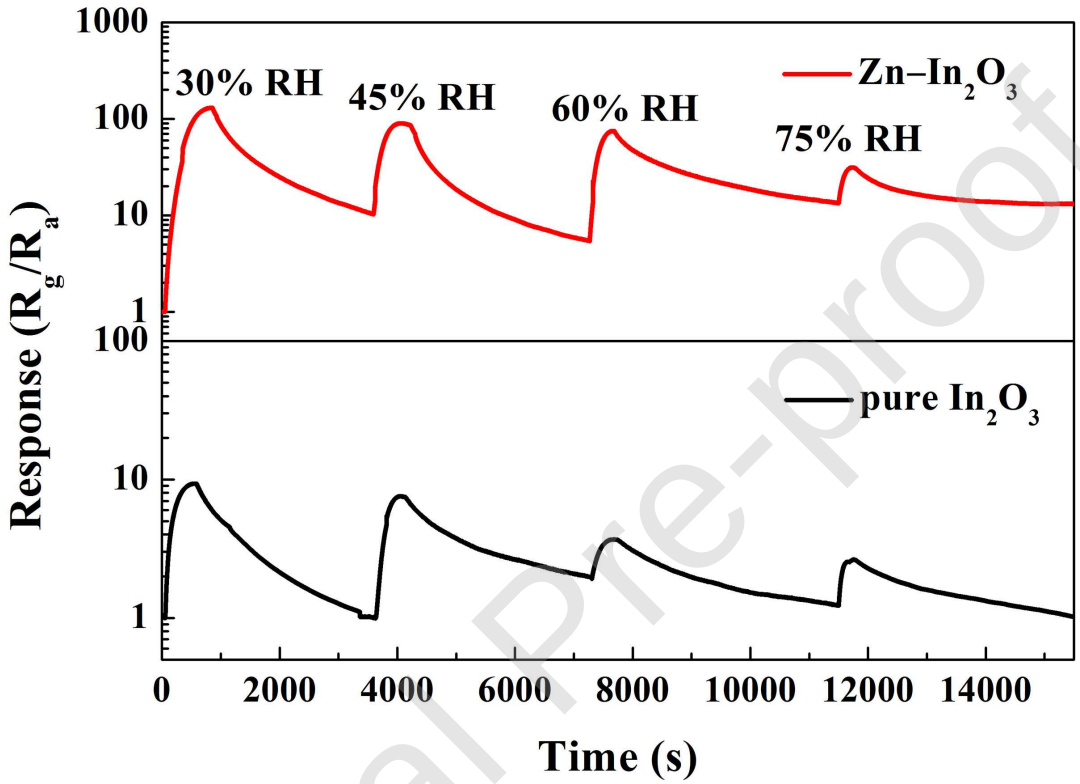

9. Fig. 9. Response–recovery curves to 5 ppm NO_2 of the two sensors at 50 °C under

various RH.

Fig. 10

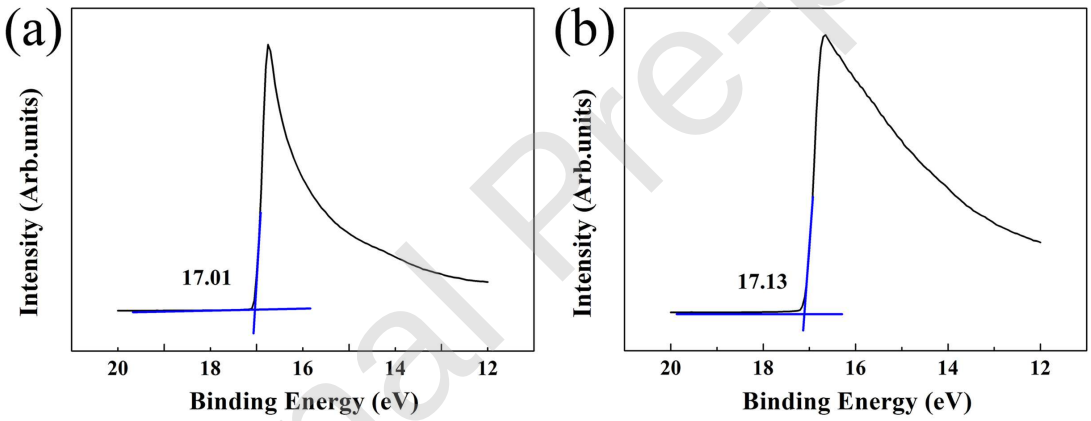

10. Fig. 10. High-binding-energy regions of UPS spectra of (a) pure In_2O_3 nanofibers and (b) Zn–In_2O_3 composite nanofibers.

Fig. 11

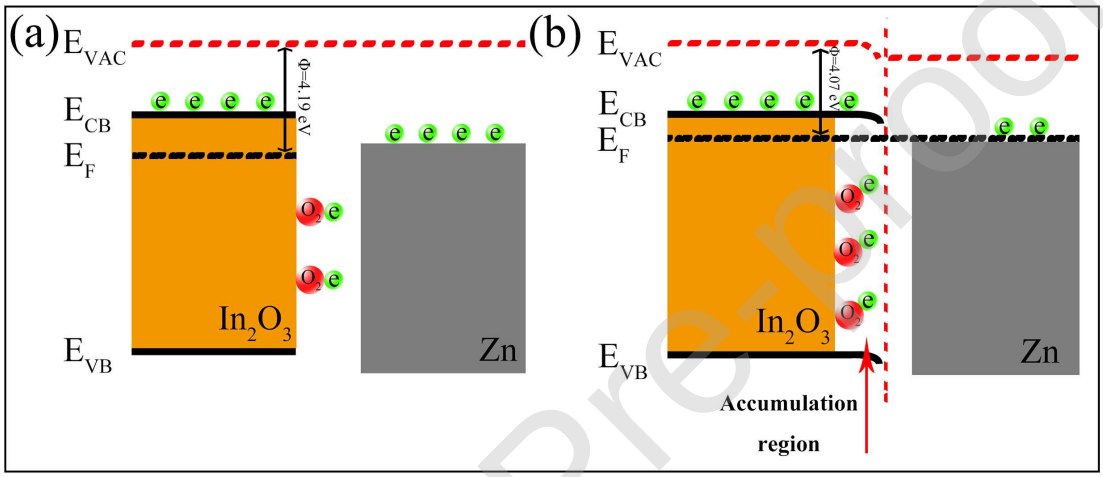

11. Fig. 11. (a) Schematic energy band diagram of In_2O_3 and Zn; (b) schematic energy band diagram and illustration of sensing mechanism for Zn–In_2O_3

heterojunction.

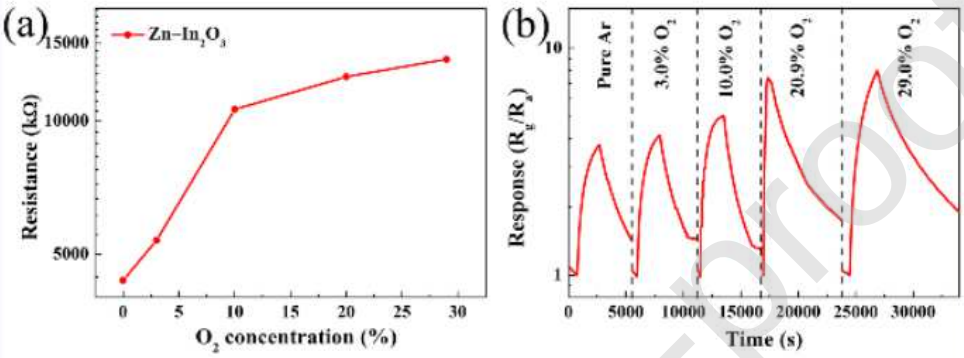

12. Fig. 12. (a) Resistances of the Zn–In_2O_3 sensor at 50 °C under various O_2 concentrations; (b) response–recovery curves of the Zn–In_2O_3 sensor to 1 ppm NO_2 at 50 °C under various O_2 concentrations.

Tables

1. Table 1. A comparison of NO_2 sensing performances between Zn–In_2O_3 nanofibers and previously reported In_2O_3-based nanostructures.

Table 1

Sensing materials	NO_2(ppm)	Temp.	Res.	Method	Ref.
In_2O_3 nanobricks	0.5	50 °C	402.0	Precipitation	[30]
Pt–decorated In_2O_3 nanorods	200	300 °C	11.0	Sol-gel method	[4]
Pt–In_2O_3 nanofibers	1	25 °C	23.9	Electrospinning	[31]
Au–modified In_2O_3 films	10	400 °C	28.0	Sputtering	[5]
Au–porous In_2O_3 powders	0.25	30 °C	~10000	Ultrasonic spray pyrolysis	[32]
Pd–loaded In_2O_3 nanowire network	5	110 °C	27.0	Electroless plating	[12]
Pd–In_2O_3 nanowires	5	300 °C	4.8	Sputtering	[18]
Pd loaded macroporous In_2O_3	0.5	25 °C	980	Reduction precipitation	[33]
Ag–In_2O_3 nanostructures	150	100 °C	1.8	Hydrothermal	[19]
Co_3O_4/In_2O_3 heterojunctions	10	150 °C	27.9	Hydrothermal	[15]

rGO–In_2O_3 nanofibers	5	50°C	42.0	Electrospinning	[34]
Zn–In_2O_3 composite nanofibers	5	50 °C	130.0	Electrospinning and thermal evaporation	This study